

## Article

# Lipid-Coated Polymeric Nanoparticles for the Photodynamic Therapy of Head and Neck Squamous Cell Carcinomas

Valeri Roschenko<sup>1</sup>, Abdallah M. Ayoub<sup>1</sup>, Konrad Engelhardt<sup>1</sup>, Jens Schäfer<sup>1</sup> , Muhammad Umair Amin<sup>1</sup>, Eduard Preis<sup>1,\*</sup> , Robert Mandic<sup>2,\*</sup>  and Udo Bakowsky<sup>1,\*</sup> 

- <sup>1</sup> Department of Pharmaceutics and Biopharmaceutics, University of Marburg, Robert-Koch-Str. 4, 35037 Marburg, Germany; valeri.roschenko@pharmazie.uni-marburg.de (V.R.); abdallah.ayoub@pharmazie.uni-marburg.de (A.M.A.); konrad.engelhardt@pharmazie.uni-marburg.de (K.E.); jens.schaefer@pharmazie.uni-marburg.de (J.S.); muhammad.umairamin@pharmazie.uni-marburg.de (M.U.A.)
- <sup>2</sup> Department of Otorhinolaryngology, Head and Neck Surgery, University Hospital Marburg, Baldingerstraße, 35033 Marburg, Germany
- \* Correspondence: eduard.preis@pharmazie.uni-marburg.de (E.P.); mandic@med.uni-marburg.de (R.M.); ubakowsky@aol.com (U.B.)

**Abstract:** Next to alcohol and tobacco abuse, infection with human papillomaviruses (HPVs) is a major risk factor for developing head and neck squamous cell carcinomas (HNSCCs), leading to 350,000 casualties worldwide each year. Limited therapy options and drug resistance raise the urge for alternative methods such as photodynamic therapy (PDT), a minimally invasive procedure used to treat HNSCC and other cancers. We prepared lipid-coated polymeric nanoparticles encapsulating curcumin as the photosensitizer (CUR-LCNPs). The prepared CUR-LCNPs were in the nanometer range ( $153.37 \pm 1.58$  nm) and showed an encapsulation efficiency of  $92.69 \pm 0.03\%$ . Proper lipid coating was visualized using atomic force microscopy (AFM). The CUR-LCNPs were tested in three HPV<sup>pos</sup> and three HPV<sup>neg</sup> HNSCC lines regarding their uptake capabilities and in vitro cell killing capacity, revealing a variable but highly significant tumor cell inhibiting effect in all tested HNSCC cell lines. No significant differences were detected between the HPV<sup>pos</sup> and HPV<sup>neg</sup> HNSCC groups (mean IC<sub>50</sub>:  $9.34 \pm 4.73$   $\mu$ mol/L vs.  $6.88 \pm 1.03$   $\mu$ mol/L), suggesting CUR-LCNPs/PDT to be a promising therapeutic option for HNSCC patients independent of their HPV status.

**Keywords:** human papillomavirus; cancer; PDT; curcumin; HNSCC; PLGA; liposomes; LED



**Citation:** Roschenko, V.; Ayoub, A.M.; Engelhardt, K.; Schäfer, J.; Amin, M.U.; Preis, E.; Mandic, R.; Bakowsky, U. Lipid-Coated Polymeric Nanoparticles for the Photodynamic Therapy of Head and Neck Squamous Cell Carcinomas.

*Pharmaceutics* **2023**, *15*, 2412.

<https://doi.org/10.3390/pharmaceutics15102412>

Academic Editor: Maria Carafa

Received: 28 August 2023

Revised: 20 September 2023

Accepted: 30 September 2023

Published: 2 October 2023



**Copyright:** © 2023 by the authors. Licensee MDPI, Basel, Switzerland. This article is an open access article distributed under the terms and conditions of the Creative Commons Attribution (CC BY) license (<https://creativecommons.org/licenses/by/4.0/>).

## 1. Introduction

Human papillomaviruses (HPVs) are categorized as a group of oncogenic factors for various malignancies, especially cervical and head and neck squamous cell carcinomas (HNSCCs), accounting for approximately 4% of all solid tumors. Additionally, HNSCCs are responsible for 1–2% of all cancer-related mortalities [1–4]. While the abuse of alcohol and smoking remains the biggest risk factor for HNSCC, approximately 30% of HNSCCs are related to HPV [5]. Yearly mortality rates for HPV-related cancers continue to rise by 2% for men and 1% for women in the United States, highlighting the need for better treatment strategies [6]. Around 80% of HNSCC cases of the oropharynx in men are attributable to HPV-16 [7]. Conventional treatment for HNSCCs involves surgery, radiation, and chemotherapy. However, these therapies may cause adverse effects such as structural deformities, scarring, and irreversible damage to normal tissues. Moreover, chemotherapy may lead to drug resistance, resulting in treatment failure and cancer recurrence [8]. Alternative treatment regimens are being explored, addressing these challenges and aiming to minimize toxicity.

Photodynamic therapy (PDT) holds great promise as an anticancer strategy. PDT is based on activating an otherwise harmless photoactive substance known as a photosensitizer using light of a specific wavelength. When combined with light and oxygen, this

photosensitizer generates reactive oxygen species (ROSs), which induce cellular damage, driving cells into apoptosis [9–11]. Among various photosensitizers, curcumin is a naturally occurring compound found in the rhizome of *Curcuma longa* L. and has recently gained much attention, as it is well known for its biocompatibility and broad pharmaceutical benefits. Despite its potential as a photosensitizer, curcumin possesses poor water solubility, requiring a suitable drug delivery system (DDS) to enhance its therapeutic efficacy [12,13]. Previous studies have reported that HPV<sup>neg</sup> HNSCCs tend to increase drug resistance and can be more challenging to treat [14,15]. More so, HPV<sup>pos</sup> HNSCCs have a better prognosis and treatment outcome after surgery, radiotherapy, and PDT. In particular, patients with HPV<sup>pos</sup> HNSCCs had a 59% reduction in risk of death from HNSCC after treatment [16–19].

In this study, we prepared curcumin-loaded lipid-coated polymeric nanoparticles (CUR-LCNPs). CUR-LCNPs consist of curcumin-loaded poly(D,L-lactid-co-glycolid) (PLGA) nanoparticles coated with liposomes (LIPOs), formed by 1,2-dipalmitoyl-sn-glycero-3-phosphocholine (DPPC) and 1,2-distearoyl-sn-glycero-3-phosphoethanolamine-N-[methoxy(polyethylene glycol)-2000] (DSPE-PEG<sub>2000</sub>). This hybrid DDS combines the advantages of LIPOs and polymeric nanoparticles, offering increased rigidity, improved uptake, and enhanced biocompatibility, minimizing drawbacks such as instabilities and drug leakage [20]. PLGA is an FDA-approved biodegradable compound widely used as a nanocarrier, while the PEGylated lipid shell can provide longer circulation time inside the body [21,22]. Next to DPPC, which is abundantly present in the mammalian cell membrane and has a phase transition temperature suitable for thermoresponsiveness of liposomes, DSPE-PEG<sub>2000</sub> can be easily modified to achieve active antibody-targeting properties [23–25]. Dynamic light scattering (DLS) and laser Doppler anemometry (LDA) were used for size distribution and surface charge analysis, respectively. Atomic force microscopy was used for morphological characterization, and in vitro cell viability was performed in six different HNSCC lines divided into two subgroups: three HPV<sup>pos</sup> HNSCC lines and three HPV<sup>neg</sup> HNSCC lines.

The primary objective of this study was to investigate whether CUR-LCNPs can effectively be deployed for the treatment of HNSCC and if there are differences in the efficacy of this treatment between HPV<sup>pos</sup> and HPV<sup>neg</sup> HNSCC cells.

## 2. Materials and Methods

### 2.1. Materials

Curcumin (95%) was purchased from Alfa Aesar (Kandel, Germany). PLGA (Purasorb PDLG 5002A) was obtained from Corbion Purac (Amsterdam, the Netherlands). The 1,2-dipalmitoyl-sn-glycero-3-phosphocholine (DPPC) and 1,2-distearoyl-sn-glycero-3-phosphoethanolamine-N-[methoxy(polyethylene glycol)-2000] (DSPE-PEG<sub>2000</sub>) were ordered from Avanti Polar Lipids (Alabaster, AL, USA). The 2',7'-dichlorofluorescein diacetate, tetramethylrhodamine ethyl ester (TMRE), and carbonyl cyanide 4-(trifluoromethoxy) phenylhydrazone (FCCP) were purchased from Abcam (Cambridge, UK). The 3-(4,5-dimethylthiazol-2-yl)-2,5-diphenyltetrazolium bromide (MTT), poly(vinyl alcohol) (PVA, Mowiol 4–88), tert-butyl hydroperoxide (TBHP), 2',7'-dichlorofluorescein diacetate (DCFH-DA), dimethyl sulfoxide (DMSO), and acetonitrile were all supplied by Sigma-Aldrich Chemie GmbH (Taufkirchen, Germany). Acetone was acquired from Fisher Scientific GmbH (Dreieich, Germany). Ultrapure water (PURELAB flex 4, ELGA LabWater, High Wycombe, UK) was used in all experiments.

### 2.2. Light Source

A prototype low-power light-emitting diode (LED) device designed to fit multiwell plates (Lumundus GmbH, Eisenach, Germany) was used for irradiation throughout the experiments. The device was set to a wavelength of 457 nm and 100 mA. Irradiation was performed for 6.5 min, resulting in a radiant exposure of 8.6 J/cm<sup>2</sup>, which was considered optimal based on previous findings on another cancer cell line [26].

### 2.3. Nanoparticle Preparation

Nanoparticles were manufactured using nanoprecipitation [27,28]. Briefly, 2.5 mg of curcumin and 100 mg of PLGA were dissolved in 10 mL of acetone. An amount of 20 mL of 0.5% PVA aqueous solution inside a 50 mL beaker was placed on a magnetic stirring plate (IKA RT 15, IKA-Werke GmbH & Co. KG, Staufen, Germany) set to 600 rpm. The curcumin acetone mixture was injected slowly into the PVA solution. The mixture was immediately protected from light and stirred until the acetone evaporated completely. Afterward, the nanoparticle suspension was adjusted with ultrapure water to 25 mL using a volumetric flask. We prepared 5 mL aliquots, lyophilized them (Christ Alpha 1–4 LSC, Martin Christ Gefriertrocknungsanlagen GmbH, Osterode am Harz, Germany), and stored them at 4 °C. Before each experiment, the lyophilized nanoparticles were redispersed in 5 mL of phosphate-buffered saline (PBS) (pH 7.4) to achieve a theoretical final curcumin concentration of 100 µg/mL. The resuspended nanoparticles were vortexed for 2 min (ZX4 Advanced IR Vortex Mixer, Usmate Velate, Italy) and sonicated for 4 min at room temperature (Elmasonic P, Elma Schmidbauer GmbH, Singen, Germany). Unloaded nanoparticles (Blank NPs) were prepared the same way, the only difference being that they did not contain curcumin.

### 2.4. Liposome (LIPO) Preparation

The LIPOs were prepared using the thin-film hydration method [29]. Briefly, DPPC and DSPE-PEG<sub>2000</sub> (95:5 mol/mol) were dissolved in a chloroform and methanol 2:1 (*v/v*) mixture. The solvents were evaporated at 41 °C with a rotary evaporator (Heidolph Hei-VAP Digital, Heidolph Instruments, Schwabach, Germany) equipped with a vacuum pump. Subsequently, the thin film was rehydrated with 1 mL PBS (pH 7.4) and mixed intensively to form the LIPOs. This liposomal dispersion was then sonicated for 15 min at 45 °C (Elmasonic P, Elma Schmidbauer GmbH, Singen, Germany). Afterward, the liposomal dispersion was extruded 11 times through a polycarbonate membrane with a pore size of 100 nm using an Avanti mini-extruder (Avanti Polar Lipids, Alabaster, AL, USA) at 45 °C to obtain unilamellar LIPOs. The LIPO dispersion was stored at 4 °C until further use.

### 2.5. Preparation of Lipid-Coated Polymeric Nanoparticles (LCNPs)

Previous studies found the optimal lipid-to-polymer ratio to be 1:100 (m/m) [30]. We formed the lipid layer on the surface of the polymeric nanoparticle with a fusion method [31]. Briefly, LIPOs were added to curcumin-loaded polymeric nanoparticles (CUR-NPs) and vortexed for 30 s. Subsequently, the mixture was sonicated for 15 min at 50 °C, resulting in lipid coating on the CUR-NPs' surface. Unloaded LCNPs were prepared the same way, the only difference being that we used PLGA nanoparticles without curcumin.

### 2.6. Particle Size and $\zeta$ -Potential

The hydrodynamic diameter and zeta potential ( $\zeta$ ) of the LIPOs, CUR-NPs, Blank NPs, CUR-LCNPs, and LCNPs were measured with dynamic light scattering (DLS) and laser doppler anemometry (LDA) using Zetasizer Nano ZS (Malvern Panalytica GmbH, Kassel, Germany). Before measurement, the samples were diluted 1:50 (*v/v*) with ultrapure water and filled into a folded capillary cell (DTS1070, Malvern Panalytical GmbH) [32]. Three independent samples were analyzed ( $n = 3$ ).

### 2.7. Encapsulation Efficiency

The encapsulation efficiency (EE) of CUR-LCNPs was determined by comparing the mass of free, non-encapsulated curcumin to the total mass of curcumin [33]. An equal volume of acetonitrile was added to the CUR-LCNPs to dissolve them and determine the total mass of curcumin. The sample was then vortexed and sonicated. Next, the sample was diluted and analyzed spectrophotometrically (Multiskan Go, Thermo Fisher Scientific, Waltham, MA, USA) at  $\lambda = 424$  nm. The mass of non-encapsulated curcumin was determined after an appropriate volume of CUR-LCNPs was centrifuged at  $2000 \times g$

(Centrifuge 5418, Eppendorf AG, Hamburg, Germany) and washed thrice with PBS (pH 7.4). Afterward, the supernatant was removed carefully, and the remaining curcumin was mixed with acetonitrile (1:1 *v/v*) and analyzed as described above. The following Equation (1) was used to calculate the encapsulation efficiency:

$$EE\% = \frac{\text{total mass of curcumin}[mg] - \text{mass of free curcumin}[mg]}{\text{total mass of curcumin}[mg]} \% \quad (1)$$

## 2.8. Atomic Force Microscopy

For AFM studies, we analyzed LIPOs, CUR-NPs, and CUR-LCNPs independently. Freshly cut silicon wafers (0.5 cm × 0.5 cm) were mounted onto a glass slide and thoroughly cleaned with isopropanol and ultrapure water. Afterward, LIPOs, CUR-NPs, and CUR-LCNPs were diluted 1:1 (*v/v*) with ultrapure water and pipetted onto the silicon wafers. Samples were then incubated for 30 min to allow adherence of the nanovesicles to the surface of the wafer. Excess water was shaken off, and samples were mounted onto the stage of NanoWizard<sup>®</sup>-3 NanoScience AFM (JPK/Bruker, Berlin, Germany), which was vibration-damped and located in an acoustic isolation chamber. The samples were measured at RT in AC mode in air. A target amplitude of 1 V was selected, and the relative setpoint was set to 90%. A commercial AFM cantilever HQ:NSC16/Al BS (MikroMasch Europe, Wetzlar, Germany) with a resonance frequency of 160 kHz and a force constant of 45 N/m was used for all measurements. Settings like gain, setpoint, and drive amplitude were adjusted during measurements to optimize the image quality. Scan speed ranged from 0.6 to 1 Hz depending on image sizes. The raw files were then edited by using JPK data processing Software 4.2. A polynomial fit was subtracted from each scan line independently by using a limited data range. Minor imaging errors were corrected by replacing lines using interpolating, and outliers were replaced using neighboring pixels [30].

## 2.9. Cell Culture

Six different cancer cell lines were included in this study. All cell lines were derived from head and neck squamous cell carcinoma (HNSCC) and can be divided into two subgroups, i.e., HPV<sup>pos</sup> and HPV<sup>neg</sup> cell lines. UM-SCC-47, UPCI-SCC-154, and UM-SCC-104 represent the HPV<sup>pos</sup> subgroup, while UM-SCC-3, UM-SCC-27, and UT-SCC-26A are the HPV<sup>neg</sup> subgroup. UM-SCC-47, UM-SCC-104, UM-SCC-3, and UM-SCC-27 were provided by Dr. Carey, University of Michigan, USA. UPCI-SCC-154 was kindly supplied by Dr. Ferris, University of Pennsylvania, USA. UT-SCC-26A cells were furnished by Dr. Grønman, University of Turku, Finland [34–36].

Cells were grown under humid conditions at 37 °C and 5% CO<sub>2</sub> (In-VitroCell ES NU-5841E, NuAire, Inc., Plymouth, MA, USA) and cultured in Dulbecco's modified Eagle's medium (DMEM, Capricorn Scientific GmbH, Ebsdorfergrund, Germany) supplemented with 10% fetal bovine serum (Sigma-Aldrich Chemie GmbH) and 1% antibiotic/antimycotic solution (100×, Capricorn Scientific GmbH). Before passaging, using Trypsin (0.05%, Cytiva HyClone™ Trypsin-Protease, Thermo Fisher Scientific) for detachment, the cells were washed with (Ca<sup>2+</sup>/Mg<sup>2+</sup> free) PBS (pH 7.4, sterile filtered). Subcultures were grown in monolayers until reaching 80% confluence.

The mouse fibroblast cell line (L929), obtained from DSMZ (Braunschweig, Germany), was used to demonstrate biocompatibility. It was cultivated similarly to the cells described above, except Roswell Park Memorial Institute (RPMI) 1640 cell culture medium was used instead of DMEM.

## 2.10. Drug Uptake Studies

### 2.10.1. Confocal Laser Scanning Microscopy (CLSM)

Confocal laser scanning microscopy (CLSM) was used to analyze the cellular accumulation of curcumin. Briefly, cells were seeded individually in 12-well plates containing cover glasses (ø 15 mm, Paul Marienfeld GmbH & Co. KG, Lauda-Königshofen, Germany) and

allowed to adhere overnight. The next day, cells were treated with 10  $\mu\text{mol/L}$  CUR-LCNP for 4 h. After incubation, the cells were washed with PBS and fixed with ROTI<sup>®</sup> Histofix 4%. Afterward, the cells were washed again and stained with 4', 6-diamidino-2-phenylindole (DAPI) for 5 min. The cells were washed again, and the cover glasses were mounted on microscope slides and fixed with FluorSave (Calbiochem Corp. San Diego, CA, USA) [28]. Images were captured using a Zeiss Axio Observer Z1 equipped with an LSM 700 confocal unit (Carl Zeiss Microscopy GmbH, Oberkochen, Germany). The samples were excited with  $\lambda_{\text{ex}} = 405 \text{ nm}$  for DAPI and  $\lambda_{\text{ex}} = 488 \text{ nm}$  for curcumin. Appropriate filters were used to obtain the images.

### 2.10.2. Flow Cytometry

Flow cytometry was executed to evaluate the curcumin uptake of all HNSCC cell lines. Therefore, HNSCC cells were seeded individually in 6-well plates at a density of  $3 \times 10^5$  cells/well and allowed to adhere overnight. Next, the cells were treated with 10  $\mu\text{mol/L}$  CUR-LCNP for 4 h. Afterward, cells were detached, washed, and resuspended in PBS. For flow cytometry, the Cytoflex LX (Beckmann Coulter GmbH, Krefeld, Germany) was utilized (Filter: B525-FITC;  $\lambda_{\text{ex}} 488 \text{ nm}/\lambda_{\text{em}} 525/40 \text{ nm}$ ). In total, 10,000 single-cell events were recorded in each measurement. FlowJo v10.6.1 was used to further process and analyze the data. Drug uptake values are calculated with the Overton algorithm and presented as percentages of total cells compared to a non-treated control of a similar cell line [37,38].

### 2.11. In Vitro Cell Viability

The different cell types were seeded individually and independently in 96-well plates (Nunclon Delta, Thermo Fisher Scientific, Waltham, MA, USA) at a density of 15,000 cells/ $0.35 \text{ cm}^2$  (per well) and were allowed to grow overnight. Afterward, the cells were incubated with the CUR-LCNPs with curcumin concentrations ranging from 50  $\mu\text{mol/L}$  to 0  $\mu\text{mol/L}$  and free curcumin (dissolved in DMSO 1%) for 4 h. After the incubation, the formulations were replaced with fresh medium and immediately irradiated with a light fluence of  $8.6 \text{ J/cm}^2$  at  $\lambda = 457 \text{ nm}$  before placing them back in the incubator for 18 h. Then, the medium was replaced by MTT reagent diluted with medium 1:10 (*v/v*) to a final MTT concentration of 0.2 mg/mL. After incubating the cells for another 4 h, the MTT reagent was replaced with DMSO to dissolve the resulting formazan crystals. The absorbance was measured using the Infinite 200 Pro microplate reader (Tecan Group AG, Männedorf, Switzerland) at  $\lambda = 570 \text{ nm}$  [39,40].

### 2.12. Biocompatibility Studies

The biocompatibility of CUR-LCNP and CUR-NP was assessed in an MTT assay performed with L929 mouse fibroblast cells. Briefly, L929 cells were seeded in 96-well plates at 15,000 cells/ $0.35 \text{ cm}^2$  (per well) and allowed to adhere overnight. Afterward, CUR-LCNP and CUR-NP were added at different concentrations ranging from 0  $\mu\text{mol/L}$  to 50  $\mu\text{mol/L}$ . After the incubation, the formulations were replaced with fresh medium and placed back in the incubator for 18 h. Then, the medium was replaced by MTT reagent diluted with medium 1:10 (*v/v*) to a final MTT concentration of 0.2 mg/mL. After incubating the cells for another 4 h, the MTT reagent was replaced with DMSO to dissolve the resulting formazan crystals. The absorbance was measured using the FLUOstar Optima microplate reader (BMG Labtech, Offenburg, Germany) at  $\lambda = 570 \text{ nm}$  [41].

### 2.13. Mitochondrial Membrane Potential

The mitochondrial membrane potential (MMP) was investigated in UM-SCC-3 cells to determine whether ROS overproduction can be associated with mitochondrial depolarization. Therefore, a TMRE stain was used to detect the PDT-induced reduction in MMP. Briefly, we seeded 15,000 cells/well in 96-well plates and allowed them to grow overnight. Subsequently, we treated the cells with 10  $\mu\text{mol/L}$  of free curcumin (dissolved in 1% DMSO) or an equal concentration of CUR-LCNPs, LCNPs, NPs, and LIPOs for 4 h.

The medium was then replaced with fresh medium. Afterward, one plate was irradiated at  $8.6 \text{ J/cm}^2$  while the other was kept in the dark. After 24 h of incubation, the cells were incubated with  $400 \text{ nmol/L}$  TMRE for 30 min. The positive control was first treated with  $50 \text{ }\mu\text{mol/L}$  FCCP for 30 min and then stained with TMRE for 30 min like the rest. Next, the cells were washed twice with PBS containing 0.2% bovine serum albumin (BSA), and then fluorescence was measured using a fluorescence spectrophotometer (FLUOstar Optima microplate reader, BMG Labtech, Offenburg, Germany) ( $\lambda_{\text{ex}} 540 \text{ nm}/\lambda_{\text{em}} 580 \text{ nm}$ ) [9].

#### 2.14. Cellular Reactive Oxygen Species (cROS)

DCFH-DA was used to quantify PDT-induced intracellular ROS generation. The cells were seeded in 24-well plates and allowed to grow overnight. The next day, cells were incubated with  $10 \text{ }\mu\text{mol/L}$  free curcumin (dissolved in 1% DMSO) or equal concentrations of CUR-LCNPs, LCNPs, NPs, and LIPOs for 4 h. The medium was then replaced with  $20 \text{ }\mu\text{mol/L}$  DCFH-DA in PBS for 45 min under the exclusion of light. Next, the cells were washed twice with PBS, and one plate was irradiated at  $8.6 \text{ J/cm}^2$  while the other plate was kept in the dark. Cells were then lysed and measured using a fluorescence spectrophotometer FLUOstar Optima microplate reader ( $\lambda_{\text{ex}} 485 \text{ nm}/\lambda_{\text{em}} 520 \text{ nm}$ ) [39].

#### 2.15. Statistical Analysis

All measurements were conducted in triplicates, and the results are presented as mean  $\pm$  standard deviation unless otherwise stated. A two-tailed Student's *t*-test was performed to identify statistically significant differences. Probability values of  $p < 0.05$  are considered significant. Statistical differences are denoted as “\*”  $p < 0.05$ , “\*\*”  $p < 0.01$ , “\*\*\*”  $p < 0.001$ , and “\*\*\*\*”  $p < 0.0001$ . GraphPad Prism 9 was used for statistical calculations.

### 3. Results and Discussion

#### 3.1. Physicochemical Characterizations

In the present study, CUR-LCNPs were prepared via a fusion method. CUR-NPs were produced using the nanoprecipitation technique. PVA was needed as a stabilizer. LIPOs were prepared via a thin-film hydration method with subsequent extrusion. A PEGylated lipid was incorporated into the formulation to provide additional stability [42,43]. The composition of prepared formulations and their physicochemical properties are displayed in Table 1. CUR-LCNPs reached a high curcumin encapsulation of  $92.69 \pm 0.03\%$ , which is excellent regarding the drug loading of 2.5% curcumin to PLGA. The hydrodynamic diameters of all formulations are in the nanometric range, and except for LIPOs, all formulations have a narrow size distribution with a PDI  $< 0.2$ . In the case of LIPOs, the higher PDI ( $0.36 \pm 0.02$ ) reveals a polydisperse size distribution. All formulations have a negative  $\zeta$ -potential, with LIPO having the highest negative  $\zeta$ -potential ( $-23.03 \pm 2.17 \text{ mV}$ ), and lipid coating slightly decreases the  $\zeta$ -potential for CUR-LCNPs and LCNPs after fusion. CUR-NPs ( $149.51 \pm 4.35 \text{ nm}$ ) show a modest increase in size compared to NPs ( $132.87 \pm 0.85 \text{ nm}$ ), which might be due to the incorporation of the highly hydrophobic curcumin. A tiny increase in hydrodynamic diameter was detected in CUR-LCNPs ( $153.37 \pm 1.58 \text{ nm}$ ) in comparison with CUR-NPs ( $149.51 \pm 4.35 \text{ nm}$ ). Given an estimated thickness of the lipid membrane of approximately 4–5 nm, our findings align with the outcomes of prior experiments by our research team [30,44].

**Table 1.** Summary of particle size (hydrodynamic diameter),  $\zeta$ -potential, polydispersity index (PDI), and encapsulation efficiency (EE) of CUR-NPs, CUR-LCNPs, NPs, LCNPs, and LIPOs. Results are listed as mean  $\pm$  standard deviation.

Formulation	Particle Size [nm]	PDI	$\zeta$ -Potential [mV]	EE [%]
CUR-NPs	$149.51 \pm 4.35$	$0.16 \pm 0.06$	$-2.72 \pm 0.31$	
CUR-LCNPs	$153.37 \pm 1.58$	$0.11 \pm 0.01$	$-3.74 \pm 0.31$	
Blank NPs	$132.87 \pm 0.85$	$0.06 \pm 0.01$	$-3.10 \pm 0.23$	$92.69 \pm 0.03$
LCNP	$134.40 \pm 2.78$	$0.08 \pm 0.02$	$-4.17 \pm 0.43$	
LIPOs	$108.08 \pm 4.48$	$0.36 \pm 0.02$	$-23.03 \pm 2.17$	

### 3.2. Atomic Force Microscopy

The particles were visualized with AFM in AC mode in air. Images were acquired in a height-measured trace, lock-in amplitude, and lock-in phase. Figures 1 and 2 show well-defined spherical shapes for LIPOs, CUR-NPs, and CUR-LCNPs. We present the data as an overview (Figures 1A,C and 2A) and as more detailed images (Figures 1B,D and 2B). Utilizing the height measurement view, we analyzed the size distribution parameters. The size agrees well with the hydrodynamic diameter obtained from DLS studies. In particular, the LIPO spheres were heterogeneous in size, in agreement with the PDI > 0.2 observed with DLS. CUR-NPs and CUR-LCNPs have a homogeneous size distribution of around 150 nm. We visualized the presence of a lipid layer on the surface of the nanoparticles, with some areas around the particle showing incomplete coverage and gaps between the coating, as indicated by the white indicator in Figure 2B. On the other hand, the indicator in Figure 1D shows a particle with a smooth surface, which further supports a successful lipid coating of the polymer particle [30,44].

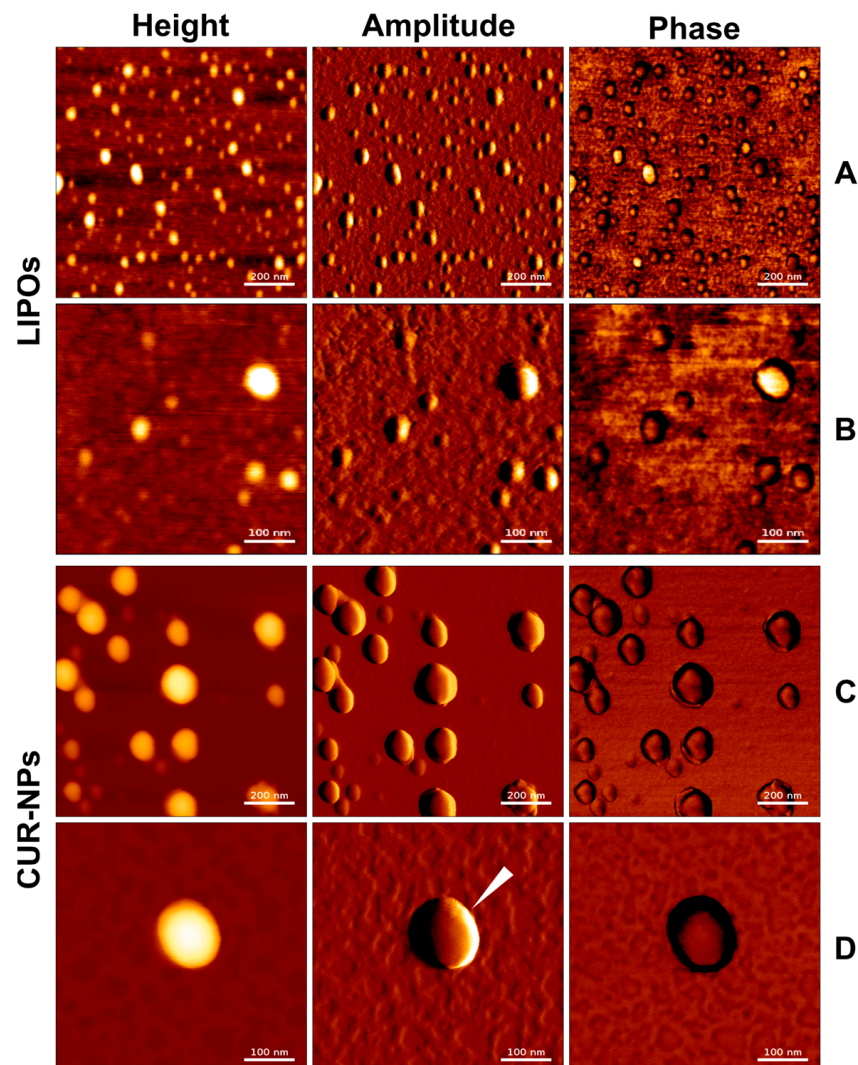


**Figure 1.** Characterization of nanoparticles by height, amplitude, and phase using atomic force microscopy. (A) and (B): LIPOs, (C) and (D): CUR-NPs with an overall smooth and even surface. Scale bars in row (A) + (C) represent 200 nm. Scale bars in row (B) + (D) represent 100 nm.

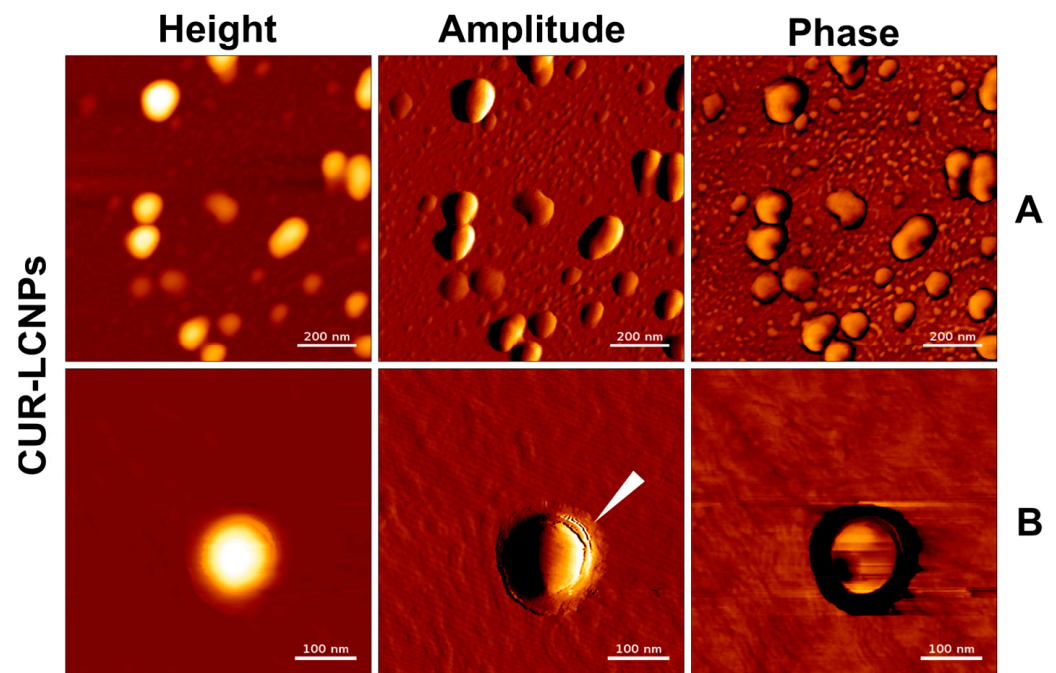


**Figure 2.** Characterization of nanoparticles by height, amplitude, and phase using atomic force microscopy. (A) and (B): CUR-LCNPs. The white arrowhead in the amplitude image in B indicates a lipid layer on the nanoparticle's surface. Scale bars in row (A) represent 200 nm. Scale bars in row (B) represent 100 nm.

### 3.3. Drug Uptake Studies

Drug uptake studies were performed to investigate the capability of CUR-LCNPs to deliver curcumin inside HNSCC cells. Figure 3 shows the merged CLSM images of cells treated with 10  $\mu\text{mol/L}$  CUR-LCNP for 4 h and DAPI staining. All cells show a pronounced curcumin fluorescence (green) in the cytosol of the cells, while DAPI has counterstained the nuclei (blue). Furthermore, flow cytometry was used to quantify the uptake of curcumin inside the HNSCC cells. All six HNSCC cell lines were treated with 10  $\mu\text{mol/L}$  CUR-LCNP for 4 h and subsequently measured, revealing reasonable uptake across all analyzed HNSCC cells (Figure 4). The uptake ranged from  $35.70\% \pm 1.86\%$  in UPCI:SCC-154 cells (HPV<sup>POS</sup>) up to  $>70\%$  in UM-SCC-3 (HPV<sup>neg</sup>), UT-SCC-26A (HPV<sup>neg</sup>), and UM-SCC-104 (HPV<sup>POS</sup>). There is no significant difference ( $p > 0.05$ ) when the mean of HPV<sup>neg</sup> ( $65.47\% \pm 12.67\%$ ) is compared to the mean of HPV<sup>POS</sup> ( $53.57\% \pm 12.69\%$ ). The results demonstrate that LCNPs are suitable to deliver highly hydrophobic curcumin to HNSCC cells, independent of their HPV status, and are in line with other studies that reported good uptake of curcumin nanoparticles [38,45]. Based on the enhanced penetration and retention effect, CUR-LCNP could provide suitable accumulation inside solid tumors [46,47].

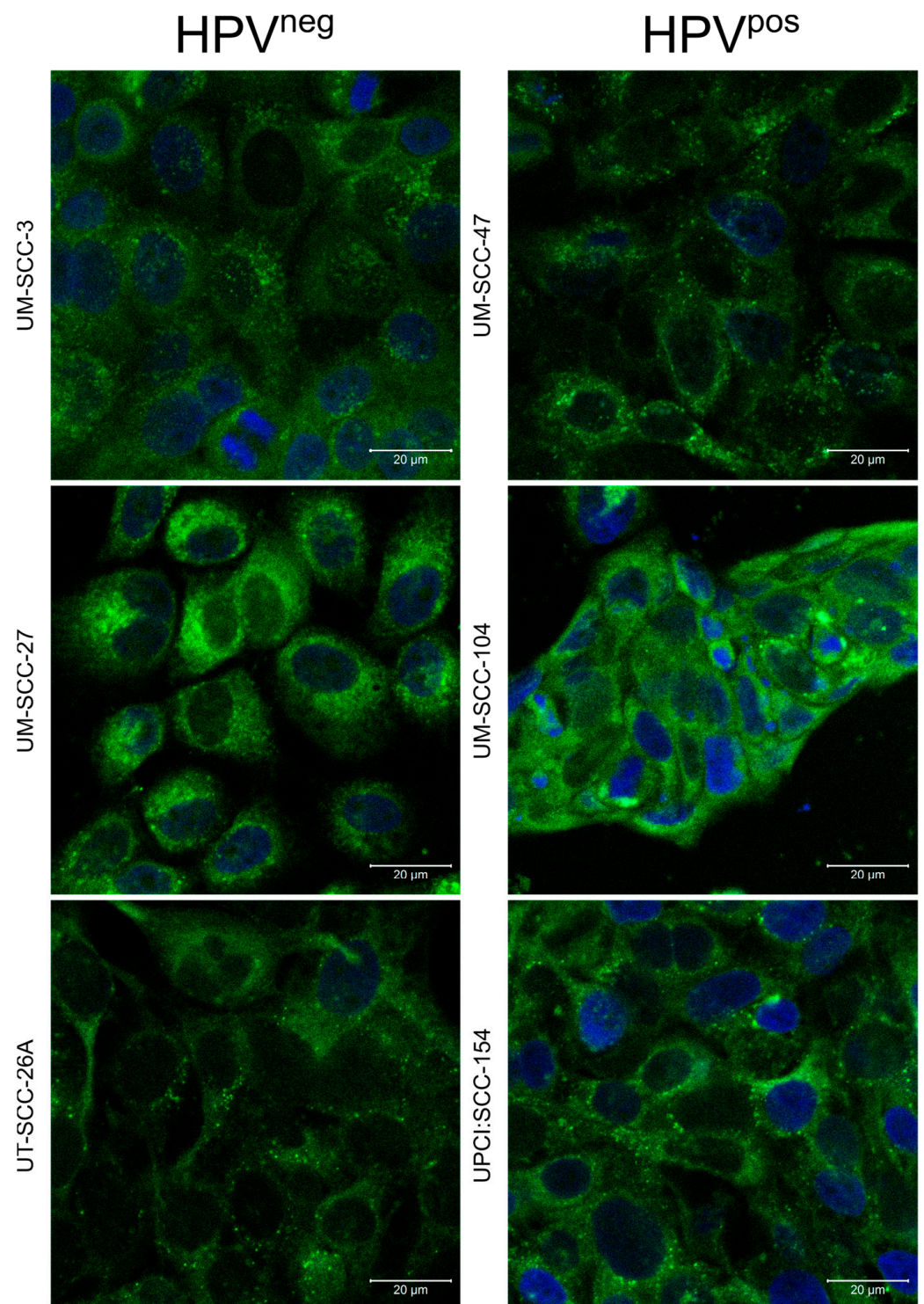


**Figure 3.** Confocal laser scanning microscope images of six different HNSCC cell lines treated for 4 h with 10 μmol/L curcumin-loaded lipid-coated polymeric nanoparticles (CUR-LCNPs). The merged images show the taken-up curcumin (green fluorescence) and DAPI-stained cell nuclei (blue fluorescence).

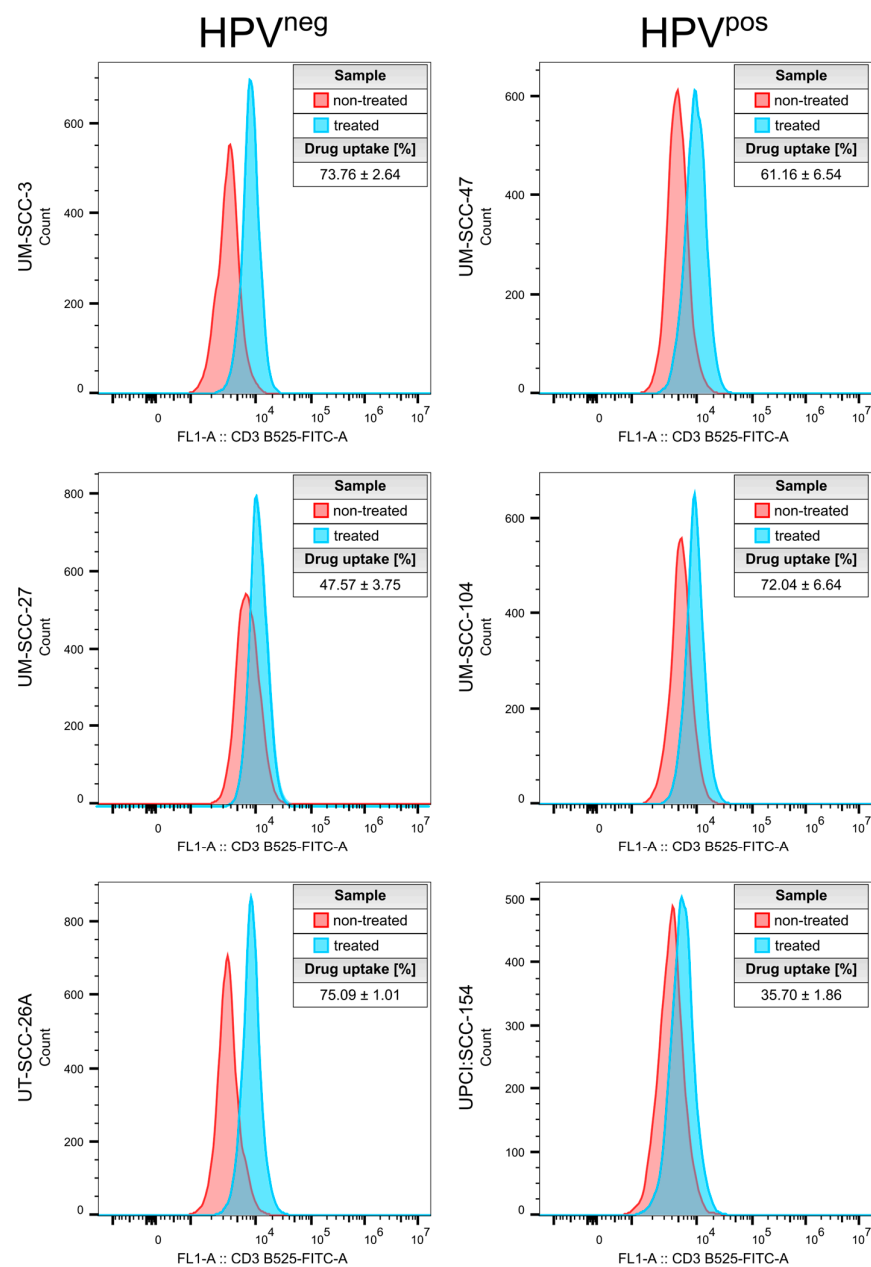


**Figure 4.** Drug uptake by flow cytometry. Treated (blue) cells were exposed to 10  $\mu\text{mol/L}$  curcumin-loaded lipid-coated polymeric nanoparticles (CUR-LCNPs) for 4 h and compared to non-treated (red) cells. Drug uptake is expressed as mean percentage  $\pm$  SD, calculated using the FlowJo Overton algorithm.

### 3.4. Effect of Photodynamic Therapy on Cell Viability

MTT assays were performed to assess *in vitro* cell viability. Cell viability is calculated by comparing the formazan absorbance of each sample with that of untreated cells. The results of all six cell lines are summarized in Figure 5. Results are split into subgroups of HPV<sup>pos</sup> and HPV<sup>neg</sup> cell lines. Furthermore, we compared CUR-LCNPs to free curcumin (dissolved in 1% DMSO) with and without irradiation (dark). The  $\text{IC}_{50}$  values are calculated via non-linear curve fitting. After 6.5 min of 100 mA irradiation at  $\lambda = 457$  nm, cells from all tested HNSCC cell lines showed a reduction in cell viability compared to their non-irradiated counterparts. Each cell line shows relatively similar sensitivity to CUR-LCNP at  $\text{IC}_{50} < 10$   $\mu\text{mol/L}$ , except for CUR-LCNP in UT-SCC-26A. UT-SCC-26A is known to be highly resistant to cisplatin and might be an exciting candidate for further investigations of new therapy strategies [48,49]. Surprisingly, at the same time, UT-SCC-26A showed the

greatest curcumin uptake of  $75.09\% \pm 1.01$ , which leads us to the suggestion that UT-SCC-26A might have a mechanism to successfully withstand different types of therapy that needs to be explored. When we compare the mean  $IC_{50}$  (Table 2) of the HPV<sup>pos</sup> subgroup with the mean  $IC_{50}$  of the HPV<sup>neg</sup> subgroup, the results show no statistically significant difference ( $p \geq 0.05$ ), allowing us to conclude that CUR-LCNP/PDT is a promising therapy option for overcoming chemotherapy or irradiation resistance in HPV<sup>neg</sup> HNSCCs [14,48,50–52]. It is worth noting that CUR-LCNP performed very similarly to free curcumin, which we see as in line with the results of our uptake studies. The cells treated with CUR-LCNPs and kept in the dark show only minor dark toxicity when the curcumin concentration is in the highest concentration tested, suggesting that photodynamic activation is key to achieving cell death. On the other hand, cells treated with free curcumin (dissolved in 1% DMSO) show more dark toxicity, which we suggest is due to the increased concentration of DMSO [53]. The results suggest that some cell lines are more sensitive to DMSO than others, with UM-SCC-27 having the greatest impact in terms of DMSO toxicity. Overall, the results show promising data for the potential use of CUR-LCNPs against HPV<sup>pos</sup> and HPV<sup>neg</sup> HNSCCs alike. CUR-LCNPs appear effective for PDT treatment of HNSCC tumors while at the same time exhibiting only minor dark toxicity. Additionally, we ranked all HNSCCs regarding their sensitivity to CUR-LCNP/PDT in Table 3.

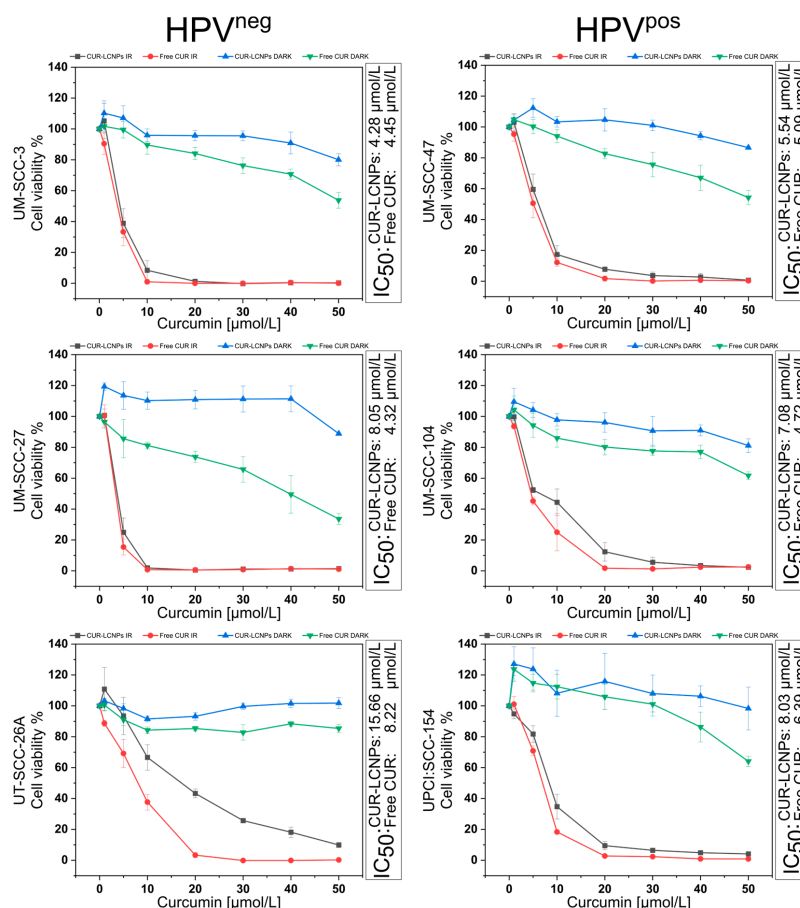


**Figure 5.** Evaluation of in vitro cell viability via MTT assay in UM-SCC-3, UM-SCC-27, and UT-SCC-26A cells (HPV<sup>neg</sup> subgroup) and UM-SCC-47, UM-SCC-104, and UPCI:SCC-154 cells (HPV<sup>pos</sup> subgroup) treated with curcumin-loaded lipid-coated polymeric nanoparticles (CUR-LCNPs) or free curcumin (Free CUR) and irradiated (IR) with  $\lambda = 457$  nm for 6.5 min, resulting in a radiant exposure of  $8.6 \text{ J/cm}^2$ , or without irradiation (DARK). The half maximal inhibitory concentration ( $IC_{50}$ ) was calculated for CUR-LCNP and free CUR (curcumin dissolved in 1% DMSO).

**Table 2.** Summary of half maximal inhibitory ( $IC_{50}$ ) concentration expressed as the mean value of the HPV<sup>pos</sup> and HPV<sup>neg</sup> subgroups treated with curcumin-loaded lipid-coated polymeric nanoparticles (CUR-LCNPs) or free curcumin (free CUR). The results are expressed as mean  $\pm$  standard deviation.

Cell Line	HPV-Status	Mean $IC_{50}$ CUR-LCNPs [ $\mu\text{mol/L}$ ]	Mean $IC_{50}$ Free CUR [ $\mu\text{mol/L}$ ]
UM-SCC-3 UM-SCC-27 UT-SCC-26A	HPV <sup>neg</sup>	9.34 $\pm$ 4.73	5.66 $\pm$ 1.81
UM-SCC-47 UM-SCC-104 UPCI:SCC-154	HPV <sup>pos</sup>	6.88 $\pm$ 1.03	5.40 $\pm$ 0.72

**Table 3.** Ranking of all HNSCCs regarding their sensitivity to curcumin-loaded lipid-coated polymeric nanoparticles (CUR-LCNPs)/PDT from highest to lowest.

CUR-LCNP/PDT Sensitivity	Cell Line	HPV-Status	$IC_{50}$ CUR-LCNPs [ $\mu\text{mol/L}$ ]
Highest  Lowest	UM-SCC-3	HPV <sup>neg</sup>	4.28
	UM-SCC-47	HPV <sup>pos</sup>	5.54
	UM-SCC-104	HPV <sup>pos</sup>	7.08
	UPCI:SCC-154	HPV <sup>pos</sup>	8.03
	UM-SCC-27	HPV <sup>neg</sup>	8.05
	UT-SCC-26A	HPV <sup>neg</sup>	15.66

### 3.5. Biocompatibility

MTT assay was performed to assess biocompatibility in L929 mouse fibroblast cells. Cell viability is calculated by comparing the formazan absorbance of each sample with that of untreated cells and is presented in Figure 6. Both CUR-LCNP and CUR-NP showed overall cell viability  $> 88\%$  and no significant differences ( $p > 0.05$ ) in cell viability. Non-irradiated CUR-LCNP also had very low dark toxicity in HNSCCs (3.3), leading us to the conclusion that CUR-LCNPs are biocompatible [54,55].

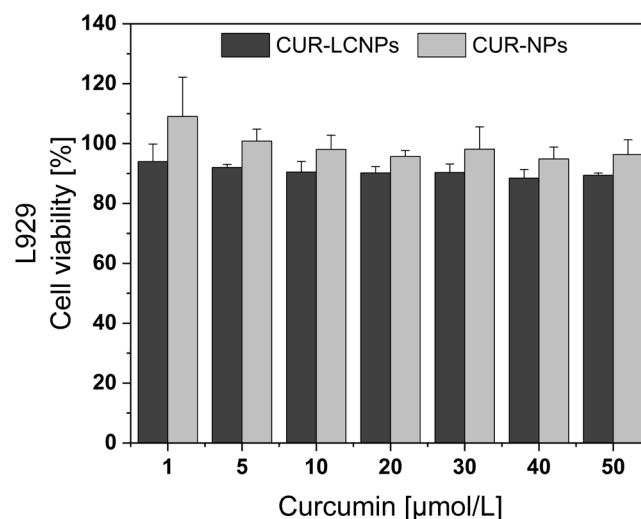


**Figure 6.** Biocompatibility of curcumin-loaded lipid-coated polymeric nanoparticles (CUR-LCNPs) and curcumin-loaded polymeric nanoparticles (CUR-NPs) with curcumin concentrations ranging from 0 to 50  $\mu\text{mol/L}$  was tested in L929 cells. Cells were kept in the dark throughout the experiment.

### 3.6. cROS

To investigate the presence of cROS generation via our photosensitizer, we performed an intracellular ROS generation assay using DCFH-DA. PDT-dependent ROS production is an inducer of apoptosis, which leads to oxidative stress and can lead to cellular apoptosis [56]. This assay was performed in UMSCC-3 cells, a well-established and representative head and neck squamous cell carcinoma cell line with reports dating back to the 1980s [57,58]. In Figure 7, CUR-LCNPs and free curcumin (dissolved in 1% DMSO) induce an extensive increase upon irradiation. In samples without irradiation, there is no noticeable increase of fluorescence and therefore no ROS generation. However, even the samples without curcumin show some increase in fluorescence, even though several previous studies reported those components have no ROS generation [26,59,60]. We suggest the assay might be too sensitive to some extent, and the light source could have an influence on this assay, as it is the only difference compared to non-irradiated samples.

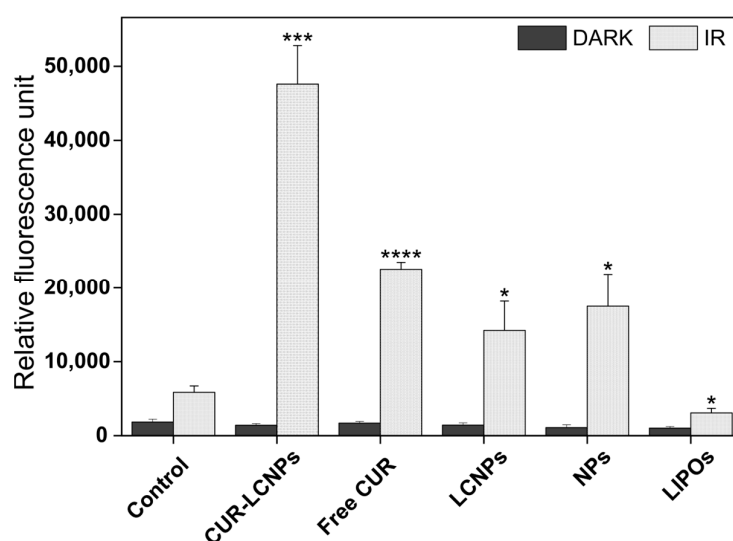


**Figure 7.** Production of reactive oxygen species inside UM-SCC-3 cells treated with PBS (control), curcumin-loaded lipid-coated polymeric nanoparticles (CUR-LCNPs), free curcumin (free CUR) (curcumin dissolved in 1% DMSO), lipid-coated polymeric nanoparticles (LCNPs), unloaded nanoparticles (NPs), and liposomes (LIPOs) and irradiated (IR) with  $\lambda = 457$  nm for 6.5 min, resulting in a radiant exposure of  $8.6 \text{ J/cm}^2$ , or without irradiation (DARK). Statistical significance is calculated with the relative fluorescence of control IR vs. the respective fluorescence of samples IR. Statistical differences are denoted as “\*”  $p < 0.05$ , “\*\*\*\*”  $p < 0.001$ , and “\*\*\*\*\*”  $p < 0.0001$ .

### 3.7. Mitochondrial Membrane Potential (MMP)

An MMP assay was performed to get more insights into the photodynamic effect. TMRE is a cationic cell-permeable dye and accumulates in the negatively charged intact mitochondrial membrane. A fully functional mitochondrial membrane has a potential of up to  $-200$  mV [61]. Changes in MMP can be a sign of mitochondrial damage and also of the cells undergoing apoptosis. These cells have reduced levels of TMRE and therefore reduced fluorescence intensity, which can be quantified considering the control. Our results (Figure 8) show that FCCP (uncoupler of oxidative phosphorylation = positive control) reduced fluorescence to  $55.34 \pm 15.22\%$  upon irradiation and  $67.83 \pm 21.85\%$  under dark conditions, while CUR-LCNP reduced fluorescence to  $18.85 \pm 6.84\%$  and free curcumin (dissolved in 1% DMSO) reduced fluorescence to  $20.29 \pm 10.20\%$  upon irradiation. There was only a minor reduction under dark conditions of  $90.47 \pm 15.90\%$  and  $93.98 \pm 19.74\%$ , respectively, suggesting high disruption of the mitochondria under irradiation. This supports the mechanism of PDT, where curcumin (photosensitizer) and light create cytotoxic ROSs that damage the cell, resulting in apoptosis [56]. Inflicting damage to

mitochondria is a well-known target of ROSs generated via PDT [59]. Some researchers even focus solely on mitochondria-targeted PDT [62].

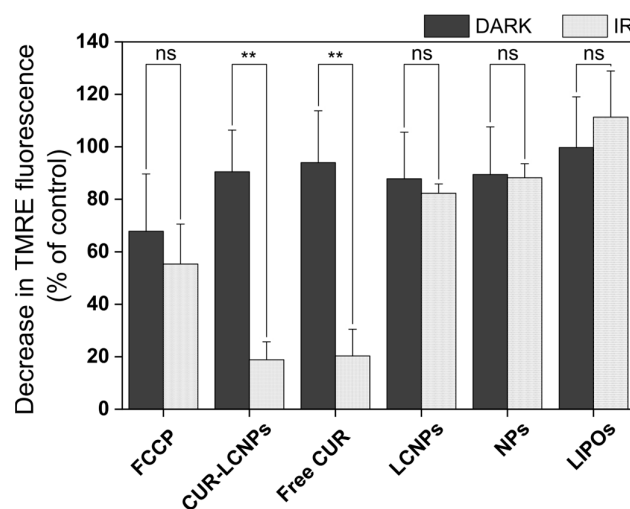


**Figure 8.** Mitochondrial transmembrane potential of UM-SCC-3 cells treated with FCCP (positive control), curcumin-loaded lipid-coated polymeric nanoparticles (CUR-LCNPs), free curcumin (free CUR) (curcumin dissolved in 1% DMSO), lipid-coated polymeric nanoparticles (LCNPs), unloaded nanoparticles (NPs), and liposomes (LIPOs) and irradiated (IR) with  $\lambda = 457$  nm for 6.5 min, resulting in a radiant exposure of  $8.6 \text{ J/cm}^2$ , or without irradiation (DARK). Results are normalized and compared to PBS as the negative control (100%). Statistical differences are denoted as “\*\*”  $p < 0.01$ .

#### 4. Conclusions

In conclusion, curcumin-loaded lipid-coated nanoparticles (CUR-LCNPs) were successfully prepared using a fusion method, achieving a high curcumin encapsulation efficiency of 92.69%. Physicochemical characterizations confirmed nanometric size and effective lipid coating. Atomic force microscopy images highlighted the well-defined spherical shape of CUR-LCNPs. Flow cytometry data showed reasonable uptake of curcumin, and the photodynamic efficacy of CUR-LCNPs was evident in inhibiting cell viability across a total of six HNSCC cell lines, both HPV<sup>pos</sup> and HPV<sup>neg</sup>, with only low dark toxicity. Biocompatibility was shown in L929 cells. Our data indicate that CUR-LCNP-based PDT is a promising minimally invasive and supportive therapeutic approach in head and neck cancer, affecting HPV<sup>pos</sup> and HPV<sup>neg</sup> cells equally.

**Author Contributions:** Conceptualization, R.M. and U.B.; data curation, J.S., M.U.A. and E.P.; formal analysis, V.R. and E.P.; funding acquisition, U.B.; investigation, V.R., A.M.A. and K.E.; methodology, V.R.; project administration, E.P., R.M. and U.B.; resources, R.M. and U.B.; supervision, E.P., R.M. and U.B.; validation, V.R. and A.M.A.; visualization, V.R. and E.P.; writing—original draft, V.R.; writing—review and editing, A.M.A., K.E., J.S., M.U.A., E.P., R.M. and U.B. All authors have read and agreed to the published version of the manuscript.

**Funding:** This work (flow cytometry) was supported by a grant from the Deutsche Forschungsgemeinschaft (project 443291381).

**Institutional Review Board Statement:** Not applicable.

**Informed Consent Statement:** Not applicable.

**Data Availability Statement:** The data presented in this study are available on request from the corresponding author.

**Acknowledgments:** The authors highly acknowledge technical support during the HNSCC cell culture from Sadowski (Research Laboratory, Department of Otorhinolaryngology, Head and Neck Surgery, University Hospital Marburg, Germany). Open Access funding was provided by the Open Access Publishing Fund of Philipps-Universität Marburg with the support of the Deutsche

Forschungsgemeinschaft (DFG, German Research Foundation). The graphical abstract was partly generated using Servier Medical Art, provided by Servier, licensed under a Creative Commons Attribution 3.0 unported license.

**Conflicts of Interest:** The authors declare no conflict of interest.

## References

1. Marziliano, A.; Teckie, S.; Diefenbach, M.A. Alcohol-related head and neck cancer: Summary of the literature. *Head Neck* **2020**, *42*, 732–738. [[CrossRef](#)] [[PubMed](#)]
2. Haring, C.T.; Bhambhani, C.; Brummel, C.; Jewell, B.; Bellile, E.; Heft Neal, M.E.; Sandford, E.; Spengler, R.M.; Bhargale, A.; Spector, M.E.; et al. Human papilloma virus circulating tumor DNA assay predicts treatment response in recurrent/metastatic head and neck squamous cell carcinoma. *Oncotarget* **2021**, *12*, 1214–1229. [[CrossRef](#)] [[PubMed](#)]
3. Ferlay, J.; Colombet, M.; Soerjomataram, I.; Mathers, C.; Parkin, D.M.; Piñeros, M.; Znaor, A.; Bray, F. Estimating the global cancer incidence and mortality in 2018: GLOBOCAN sources and methods. *Int. J. Cancer* **2019**, *144*, 1941–1953. [[CrossRef](#)] [[PubMed](#)]
4. Sabatini, M.E.; Chiocca, S. Human papillomavirus as a driver of head and neck cancers. *Br. J. Cancer* **2020**, *122*, 306–314. [[CrossRef](#)] [[PubMed](#)]
5. Panwar, A.; Batra, R.; Lydiatt, W.M.; Ganti, A.K. Human papilloma virus positive oropharyngeal squamous cell carcinoma: A growing epidemic. *Cancer Treat. Rev.* **2014**, *40*, 215–219. [[CrossRef](#)] [[PubMed](#)]
6. Siegel, R.L.; Miller, K.D.; Wagle, N.S.; Jemal, A. Cancer statistics, 2023. *CA Cancer J. Clin.* **2023**, *73*, 17–48. [[CrossRef](#)] [[PubMed](#)]
7. Liao, C.-I.; Francoeur, A.A.; Kapp, D.S.; Caesar, M.A.P.; Huh, W.K.; Chan, J.K. Trends in Human Papillomavirus-Associated Cancers, Demographic Characteristics, and Vaccinations in the US, 2001–2017. *JAMA Netw. Open* **2022**, *5*, e222530. [[CrossRef](#)] [[PubMed](#)]
8. Vermorken, J.B.; Specenier, P. Optimal treatment for recurrent/metastatic head and neck cancer. *Ann. Oncol.* **2010**, *21* (Suppl. 7), vii252–vii261. [[CrossRef](#)]
9. Ayan, S.; Gunaydin, G.; Yesilgul-Mehmetcik, N.; Gedik, M.E.; Seven, O.; Akkaya, E.U. Proof-of-principle for two-stage photodynamic therapy: Hypoxia triggered release of singlet oxygen. *Chem. Commun.* **2020**, *56*, 14793–14796. [[CrossRef](#)]
10. Yoo, J.-O.; Ha, K.-S. New insights into the mechanisms for photodynamic therapy-induced cancer cell death. *Int. Rev. Cell Mol. Biol.* **2012**, *295*, 139–174. [[CrossRef](#)]
11. Gutberlet, B.; Preis, E.; Roschenko, V.; Bakowsky, U. Photothermally Controlled Drug Release of Poly(D,L-lactide) Nanofibers Loaded with Indocyanine Green and Curcumin for Efficient Antimicrobial Photodynamic Therapy. *Pharmaceutics* **2023**, *15*, 327. [[CrossRef](#)] [[PubMed](#)]
12. Mohanty, C.; Das, M.; Sahoo, S.K. Emerging role of nanocarriers to increase the solubility and bioavailability of curcumin. *Expert Opin. Drug Deliv.* **2012**, *9*, 1347–1364. [[CrossRef](#)] [[PubMed](#)]
13. Giordano, A.; Tommonaro, G. Curcumin and Cancer. *Nutrients* **2019**, *11*, 2376. [[CrossRef](#)] [[PubMed](#)]
14. Nagel, R.; Martens-de Kemp, S.R.; Buijze, M.; Jacobs, G.; Braakhuis, B.J.M.; Brakenhoff, R.H. Treatment response of HPV-positive and HPV-negative head and neck squamous cell carcinoma cell lines. *Oral Oncol.* **2013**, *49*, 560–566. [[CrossRef](#)] [[PubMed](#)]
15. Ang, K.K.; Harris, J.; Wheeler, R.; Weber, R.; Rosenthal, D.I.; Nguyen-Tân, P.F.; Westra, W.H.; Chung, C.H.; Jordan, R.C.; Lu, C.; et al. Human papillomavirus and survival of patients with oropharyngeal cancer. *N. Engl. J. Med.* **2010**, *363*, 24–35. [[CrossRef](#)] [[PubMed](#)]
16. Cho, W.J.; Kessel, D.; Rakowski, J.; Loughery, B.; Najy, A.J.; Pham, T.; Kim, S.; Kwon, Y.T.; Kato, I.; Kim, H.E.; et al. Photodynamic Therapy as a Potent Radiosensitizer in Head and Neck Squamous Cell Carcinoma. *Cancers* **2021**, *13*, 1193. [[CrossRef](#)] [[PubMed](#)]
17. D’Souza, G.; McNeel, T.S.; Fakhry, C. Understanding personal risk of oropharyngeal cancer: Risk-groups for oncogenic oral HPV infection and oropharyngeal cancer. *Ann. Oncol.* **2017**, *28*, 3065–3069. [[CrossRef](#)] [[PubMed](#)]
18. Gillison, M.L.; Koch, W.M.; Capone, R.B.; Spafford, M.; Westra, W.H.; Wu, L.; Zahurak, M.L.; Daniel, R.W.; Viglione, M.; Symer, D.E.; et al. Evidence for a causal association between human papillomavirus and a subset of head and neck cancers. *J. Natl. Cancer Inst.* **2000**, *92*, 709–720. [[CrossRef](#)]
19. Machiels, J.-P.; René Leemans, C.; Golusinski, W.; Grau, C.; Licitra, L.; Gregoire, V. Squamous cell carcinoma of the oral cavity, larynx, oropharynx and hypopharynx: EHSN-ESMO-ESTRO Clinical Practice Guidelines for diagnosis, treatment and follow-up. *Ann. Oncol.* **2020**, *31*, 1462–1475. [[CrossRef](#)]
20. Wilhelm Romero, K.; Quirós, M.I.; Vargas Huertas, F.; Vega-Baudrit, J.R.; Navarro-Hoyos, M.; Araya-Sibaja, A.M. Design of Hybrid Polymeric-Lipid Nanoparticles Using Curcumin as a Model: Preparation, Characterization, and In Vitro Evaluation of Demethoxycurcumin and Bisdemethoxycurcumin-Loaded Nanoparticles. *Polymers* **2021**, *13*, 4207. [[CrossRef](#)]
21. Wang, Y.; Qin, B.; Xia, G.; Choi, S.H. FDA’s Poly (Lactic-Co-Glycolic Acid) Research Program and Regulatory Outcomes. *AAPS J.* **2021**, *23*, 92. [[CrossRef](#)] [[PubMed](#)]
22. Fan, W.; Peng, H.; Yu, Z.; Wang, L.; He, H.; Ma, Y.; Qi, J.; Lu, Y.; Wu, W. The long-circulating effect of pegylated nanoparticles revisited via simultaneous monitoring of both the drug payloads and nanocarriers. *Acta Pharm. Sin. B* **2022**, *12*, 2479–2493. [[CrossRef](#)] [[PubMed](#)]
23. Kowalska, M.; Broniatowski, M.; Mach, M.; Płachta, Ł.; Wydro, P. The effect of the polyethylene glycol chain length of a lipopolymer (DSPE-PEGn) on the properties of DPPC monolayers and bilayers. *J. Mol. Liq.* **2021**, *335*, 116529. [[CrossRef](#)]

24. Huang, S.; Zhang, H.; Zhang, Y.; Wang, L.; Zhang, Z.; Zhang, L. Comparison of two methods for tumour-targeting peptide modification of liposomes. *Acta Pharmacol. Sin.* **2023**, *44*, 832–840. [[CrossRef](#)] [[PubMed](#)]
25. Dayyih, A.A.; Gutberlet, B.; Preis, E.; Engelhardt, K.H.; Amin, M.U.; Abdelsalam, A.M.; Bonsu, M.; Bakowsky, U. Thermoresponsive Liposomes for Photo-Triggered Release of Hypericin Cyclodextrin Inclusion Complex for Efficient Antimicrobial Photodynamic Therapy. *ACS Appl. Mater. Interfaces* **2022**, *14*, 31525–31540. [[CrossRef](#)] [[PubMed](#)]
26. Duse, L.; Agel, M.R.; Pinnapireddy, S.R.; Schäfer, J.; Selo, M.A.; Ehrhardt, C.; Bakowsky, U. Photodynamic Therapy of Ovarian Carcinoma Cells with Curcumin-Loaded Biodegradable Polymeric Nanoparticles. *Pharmaceutics* **2019**, *11*, 282. [[CrossRef](#)] [[PubMed](#)]
27. Yallapu, M.M.; Gupta, B.K.; Jaggi, M.; Chauhan, S.C. Fabrication of curcumin encapsulated PLGA nanoparticles for improved therapeutic effects in metastatic cancer cells. *J. Colloid Interface Sci.* **2010**, *351*, 19–29. [[CrossRef](#)]
28. Raschpichler, M.; Preis, E.; Pinnapireddy, S.R.; Baghdan, E.; Pourasghar, M.; Schneider, M.; Bakowsky, U. Photodynamic inactivation of circulating tumor cells: An innovative approach against metastatic cancer. *Eur. J. Pharm. Biopharm.* **2020**, *157*, 38–46. [[CrossRef](#)]
29. Zhang, H. Thin-Film Hydration Followed by Extrusion Method for Liposome Preparation. *Methods Mol. Biol.* **2017**, *1522*, 17–22. [[CrossRef](#)]
30. Ali, S.; Amin, M.U.; Tariq, I.; Sohail, M.F.; Ali, M.Y.; Preis, E.; Ambreen, G.; Pinnapireddy, S.R.; Jedelská, J.; Schäfer, J.; et al. Lipoparticles for Synergistic Chemo-Photodynamic Therapy to Ovarian Carcinoma Cells: In vitro and in vivo Assessments. *Int. J. Nanomed.* **2021**, *16*, 951–976. [[CrossRef](#)]
31. Mandal, B.; Bhattacharjee, H.; Mittal, N.; Sah, H.; Balabathula, P.; Thoma, L.A.; Wood, G.C. Core-shell-type lipid-polymer hybrid nanoparticles as a drug delivery platform. *Nanomedicine* **2013**, *9*, 474–491. [[CrossRef](#)] [[PubMed](#)]
32. Brum, A.A.S.; Santos, P.P.d.; Da Silva, M.M.; Paese, K.; Guterres, S.S.; Costa, T.M.H.; Pohlmann, A.R.; Jablonski, A.; Flôres, S.H.; Rios, A.d.O. Lutein-loaded lipid-core nanocapsules: Physicochemical characterization and stability evaluation. *Colloids Surf. A Physicochem. Eng. Asp.* **2017**, *522*, 477–484. [[CrossRef](#)]
33. Preis, E.; Baghdan, E.; Agel, M.R.; Anders, T.; Pourasghar, M.; Schneider, M.; Bakowsky, U. Spray dried curcumin loaded nanoparticles for antimicrobial photodynamic therapy. *Eur. J. Pharm. Biopharm.* **2019**, *142*, 531–539. [[CrossRef](#)] [[PubMed](#)]
34. Mandic, R.; Schamberger, C.J.; Müller, J.F.; Geyer, M.; Zhu, L.; Carey, T.E.; Grénman, R.; Dünne, A.A.; Werner, J.A. Reduced cisplatin sensitivity of head and neck squamous cell carcinoma cell lines correlates with mutations affecting the COOH-terminal nuclear localization signal of p53. *Clin. Cancer Res.* **2005**, *11*, 6845–6852. [[CrossRef](#)] [[PubMed](#)]
35. Tang, A.L.; Hauff, S.J.; Owen, J.H.; Graham, M.P.; Czerwinski, M.J.; Park, J.J.; Walline, H.; Papagerakis, S.; Stoerker, J.; McHugh, J.B.; et al. UM-SCC-104: A new human papillomavirus-16-positive cancer stem cell-containing head and neck squamous cell carcinoma cell line. *Head Neck* **2012**, *34*, 1480–1491. [[CrossRef](#)] [[PubMed](#)]
36. Göttgens, E.-L.; Ansems, M.; Leenders, W.P.J.; Bussink, J.; Span, P.N. Genotyping and Characterization of HPV Status, Hypoxia, and Radiosensitivity in 22 Head and Neck Cancer Cell Lines. *Cancers* **2021**, *13*, 1069. [[CrossRef](#)] [[PubMed](#)]
37. Wang, J.; Kang, Y.-X.; Pan, W.; Lei, W.; Feng, B.; Wang, X.-J. Enhancement of Anti-Inflammatory Activity of Curcumin Using Phosphatidylserine-Containing Nanoparticles in Cultured Macrophages. *Int. J. Mol. Sci.* **2016**, *17*, 969. [[CrossRef](#)]
38. Punfa, W.; Yodkeeree, S.; Pitchakarn, P.; Ampasavate, C.; Limtrakul, P. Enhancement of cellular uptake and cytotoxicity of curcumin-loaded PLGA nanoparticles by conjugation with anti-P-glycoprotein in drug resistance cancer cells. *Acta Pharmacol. Sin.* **2012**, *33*, 823–831. [[CrossRef](#)]
39. Escobar, P.; Vera, A.M.; Neira, L.F.; Velásquez, A.O.; Carreño, H. Photodynamic therapy using ultradeformable liposomes loaded with chlorine aluminum phthalocyanine against *L. (V.) braziliensis* experimental models. *Exp. Parasitol.* **2018**, *194*, 45–52. [[CrossRef](#)]
40. Ambreen, G.; Duse, L.; Tariq, I.; Ali, U.; Ali, S.; Pinnapireddy, S.R.; Bette, M.; Bakowsky, U.; Mandic, R. Sensitivity of Papilloma Virus-Associated Cell Lines to Photodynamic Therapy with Curcumin-Loaded Liposomes. *Cancers* **2020**, *12*, 3278. [[CrossRef](#)]
41. Guo, L.; Chen, B.; Liu, R.; Xia, G.; Wang, Y.; Li, X.; Wei, C.; Wang, X.; Jiang, H. Biocompatibility Assessment of Polyethylene Glycol-Poly L-Lysine-Poly Lactic-Co-Glycolic Acid Nanoparticles In Vitro and In Vivo. *J. Nanosci. Nanotechnol.* **2015**, *15*, 3710–3719. [[CrossRef](#)] [[PubMed](#)]
42. Mahmoudzadeh, M.; Magarkar, A.; Koivuniemi, A.; Róg, T.; Bunker, A. Mechanistic Insight into How PEGylation Reduces the Efficacy of pH-Sensitive Liposomes from Molecular Dynamics Simulations. *Mol. Pharm.* **2021**, *18*, 2612–2621. [[CrossRef](#)] [[PubMed](#)]
43. Nosova, A.S.; Koloskova, O.O.; Nikonova, A.A.; Simonova, V.A.; Smirnov, V.V.; Kudlay, D.; Khaitov, M.R. Diversity of PEGylation methods of liposomes and their influence on RNA delivery. *MedChemComm* **2019**, *10*, 369–377. [[CrossRef](#)] [[PubMed](#)]
44. Schäfer, J.; Sitterberg, J.; Ehrhardt, C.; Kumar, M.R.; Bakowsky, U. A New Drug Vehicle—Lipid Coated Biodegradable Nanoparticles. In *Biomedical Applications of Smart Materials*; CIMTEC 2008; Trans Tech Publications Ltd.: Zurich, Switzerland, 2008; pp. 148–153.
45. Liu, J.; Xu, L.; Liu, C.; Zhang, D.; Wang, S.; Deng, Z.; Lou, W.; Xu, H.; Bai, Q.; Ma, J. Preparation and characterization of cationic curcumin nanoparticles for improvement of cellular uptake. *Carbohydr. Polym.* **2012**, *90*, 16–22. [[CrossRef](#)] [[PubMed](#)]
46. Keereweer, S.; Mol, I.M.; Kerrebijn, J.D.F.; van Driel, P.B.A.A.; Xie, B.; Baatenburg de Jong, R.J.; Vahrmeijer, A.L.; Löwik, C.W.G.M. Targeting integrins and enhanced permeability and retention (EPR) effect for optical imaging of oral cancer. *J. Surg. Oncol.* **2012**, *105*, 714–718. [[CrossRef](#)] [[PubMed](#)]

47. Zhang, Y.; Dong, P.; Yang, L. The role of nanotherapy in head and neck squamous cell carcinoma by targeting tumor microenvironment. *Front. Immunol.* **2023**, *14*, 1189323. [[CrossRef](#)] [[PubMed](#)]
48. Mandic, R.; Rodgarkia-Dara, C.J.; Krohn, V.; Wiegand, S.; Grénman, R.; Werner, J.A. Cisplatin resistance of the HNSCC cell line UT-SCC-26A can be overcome by stimulation of the EGF-receptor. *Anticancer Res.* **2009**, *29*, 1181–1187. [[PubMed](#)]
49. Tonigold, M.; Rossmann, A.; Meinold, M.; Bette, M.; Märken, M.; Henkenius, K.; Bretz, A.C.; Giel, G.; Cai, C.; Rodepeter, F.R.; et al. A cisplatin-resistant head and neck cancer cell line with cytoplasmic p53(mut) exhibits ATP-binding cassette transporter upregulation and high glutathione levels. *J. Cancer Res. Clin. Oncol.* **2014**, *140*, 1689–1704. [[CrossRef](#)]
50. Padilla, L.A.; Leung, B.S.; Carson, L.F. Evidence of an association between human papillomavirus and impaired chemotherapy-induced apoptosis in cervical cancer cells. *Gynecol. Oncol.* **2002**, *85*, 59–66. [[CrossRef](#)]
51. Reid, P.; Staudacher, A.H.; Marcu, L.G.; Olver, I.; Moghaddasi, L.; Brown, M.P.; Bezak, E. Influence of the human papillomavirus on the radio-responsiveness of cancer stem cells in head and neck cancers. *Sci. Rep.* **2020**, *10*, 2716. [[CrossRef](#)]
52. Spanos, W.C.; Nowicki, P.; Lee, D.W.; Hoover, A.; Hostager, B.; Gupta, A.; Anderson, M.E.; Lee, J.H. Immune response during therapy with cisplatin or radiation for human papillomavirus-related head and neck cancer. *Arch. Otolaryngol. Head Neck Surg.* **2009**, *135*, 1137–1146. [[CrossRef](#)] [[PubMed](#)]
53. Pal, R.; Mamidi, M.K.; Das, A.K.; Bhonde, R. Diverse effects of dimethyl sulfoxide (DMSO) on the differentiation potential of human embryonic stem cells. *Arch. Toxicol.* **2012**, *86*, 651–661. [[CrossRef](#)] [[PubMed](#)]
54. Crawford, L.; Wyatt, M.; Bryers, J.; Ratner, B. Biocompatibility Evolves: Phenomenology to Toxicology to Regeneration. *Adv. Healthc. Mater.* **2021**, *10*, e2002153. [[CrossRef](#)] [[PubMed](#)]
55. Iranshahy, M.; Hanafi-Bojd, M.Y.; Aghili, S.H.; Iranshahi, M.; Nabavi, S.M.; Saberi, S.; Filosa, R.; Nezhad, I.F.; Hasanpour, M. Curcumin-loaded mesoporous silica nanoparticles for drug delivery: Synthesis, biological assays and therapeutic potential—A review. *RSC Adv.* **2023**, *13*, 22250–22267. [[CrossRef](#)] [[PubMed](#)]
56. Turan, I.S.; Yildiz, D.; Turksoy, A.; Gunaydin, G.; Akkaya, E.U. A Bifunctional Photosensitizer for Enhanced Fractional Photodynamic Therapy: Singlet Oxygen Generation in the Presence and Absence of Light. *Angew. Chem. Int. Ed.* **2016**, *55*, 2875–2878. [[CrossRef](#)] [[PubMed](#)]
57. Baker, S.R. An in vivo model for squamous cell carcinoma of the head and neck. *Laryngoscope* **1985**, *95*, 43–56. [[CrossRef](#)] [[PubMed](#)]
58. Grenman, R.; Virolainen, E.; Shapira, A.; Carey, T. In vitro effects of tamoxifen on UM-SCC head and neck cancer cell lines: Correlation with the estrogen and progesterone receptor content. *Int. J. Cancer* **1987**, *39*, 77–81. [[CrossRef](#)]
59. Platel, A.; Carpentier, R.; Becart, E.; Mordacq, G.; Betbeder, D.; Nessler, F. Influence of the surface charge of PLGA nanoparticles on their in vitro genotoxicity, cytotoxicity, ROS production and endocytosis. *J. Appl. Toxicol.* **2016**, *36*, 434–444. [[CrossRef](#)]
60. Ricci-Júnior, E.; Marchetti, J.M. Zinc(II) phthalocyanine loaded PLGA nanoparticles for photodynamic therapy use. *Int. J. Pharm.* **2006**, *310*, 187–195. [[CrossRef](#)]
61. Teodoro, J.S.; Palmeira, C.M.; Rolo, A.P. Mitochondrial Membrane Potential ( $\Delta\Psi$ ) Fluctuations Associated with the Metabolic States of Mitochondria. In *Mitochondrial Bioenergetics*; Humana Press: New York, NY, USA, 2018; pp. 109–119.
62. Gu, X.; Shen, C.; Li, H.; Goldys, E.M.; Deng, W. X-ray induced photodynamic therapy (PDT) with a mitochondria-targeted liposome delivery system. *J. Nanobiotechnol.* **2020**, *18*, 87. [[CrossRef](#)]

**Disclaimer/Publisher's Note:** The statements, opinions and data contained in all publications are solely those of the individual author(s) and contributor(s) and not of MDPI and/or the editor(s). MDPI and/or the editor(s) disclaim responsibility for any injury to people or property resulting from any ideas, methods, instructions or products referred to in the content.